DFT Simulation of the Vibrational Spectrum of Cholesteryl Esters: A New Physical Therapy Proposal for Targeted Clearance of Atherosclerotic Lipid Plaques

Yitong Wang , Peilin Li , Haoxin Ren , Yining Li , Yawen Li , Yuqi Xia , Jingyu Zhang , Peng Zhang *

Posted Date: 7 May 2025

doi: 10.20944/preprints202505.0475.v1

Keywords: Cholesteryl ester; DFT; IR; Raman; vibrational mode; PPRA

 doi:10.20944/preprints202505.0475.v1

Article

DFT Simulation of the Vibrational Spectrum of Cholesteryl Esters: A New Physical Therapy Proposal for Targeted Clearance of Atherosclerotic Lipid Plaques

Yitong Wang [1,2,3], Peilin Li [2,3], Haoxin Ren [2], Yining Li [2], Yawen Li [2], Yuqi Xia [2], Jingyu Zhang [3] and Peng Zhang [1,*]

[1] Shandong Provincial Key Laboratory of Nuclear Science, Nuclear Energy Technology and Comprehensive Utilization, Weihai Frontier Innovation Institute of Nuclear Technology, Shandong University, Weihai 264209, China

[2] School of Space Science and Technology, Shandong University, Weihai 264209, China

[3] SDU-ANU Joint Science College, Shandong University, Weihai 264209, China

* Correspondence: zhangpeng@sdu.edu.cn; Tel.: +86-631-568-8751

Abstract: Cholesteryl ester deposition in atherosclerosis (AS) plaques drives lipid core formation and plaque instability. Traditional statin drugs lack targeting and cause adverse reactions in some patients. This study proposed a novel laser-targeted therapy strategy based on photon-phonon resonant absorption (PPRA). We assigned the vibrational modes of four cholesteryl esters: cholesteryl linoleate (CLA), cholesteryl oleate (COA), cholesteryl palmitate (CPA), and cholesteryl stearate (CSA) using first-principles density functional theory, and determined the C=O vibration frequencies ($1720-1750\ \mathrm{cm}^{-1}$). We suggested using a 52 THz laser to selectively excite C=O bond resonance, thereby achieving effective PPRA. It is predicted to disrupt cholesterol ester intermolecular hydrogen bonds, induce solid or liquid crystalline to liquid phase transitions in lipid cores. Consequently, this enhances the efficiency of esterase hydrolysis and promotes cholesterol reverse transport, which helps alleviate lipid plaque deposition. This method overcomes traditional drug limitations and offers a new physical intervention for laser-targeted therapy of AS.

Keywords: cholesteryl ester; DFT; IR; raman; vibrational mode; PPRA

1. Introduction

Atherosclerosis (AS), the primary pathological basis of cardiovascular diseases, starts with endothelial dysfunction, accompanied by abnormal lipid deposition and amplified chronic inflammation [1–3]. The dynamic deposition of low-density lipoprotein (LDL) in the vascular wall is a key pathogenic factor. Cholesteryl ester, the esterified forms of cholesterol stored in LDL, constitute a major component of the LDL lipid core and directly drive the AS lesion progression. After endothelial damage, LDL lipids infiltrate the intima, oxidizing into pro-inflammatory oxLDL in oxidative stress and acidic environments. Monocytes migrate to the arterial intima, differentiating into macrophages that engulf oxLDL through scavenger receptors [4]. Macrophages upregulate scavenger receptors and downregulate cholesterol transporters, causing cholesterol and cholesteryl ester deposition in pathological states, inflammation and foam cell formation, which are the early signs of AS [5,6]. Consequently, foam cell apoptosis or necrosis creates a growing necrotic core of cholesteryl esters, cholesterol crystals, and debris, thereby increasing vascular lesion and rupture risks [7].

AS results from various factors, both hereditary and environmental. Unhealthy lifestyles, including high-fat diets, smoking, chronic stress, and irregular sleep patterns, are widely linked to a higher AS incidence [8]. Current treatments mainly involve statins and PCSK9 inhibitors, combined

 doi:10.20944/preprints202505.0475.v1

with anti-inflammatory therapy [9–11]. However, these traditional methods lack targeting specificity. Also, some patients are resistant to or have adverse reactions to statins [9,12]. Nanocarriers, which can passively accumulate at the lesion by Enhanced Permeation and Retention (EPR) effect or actively target specific receptor by precise surface modification, have gained significant attention [13–16]. Gao's team developed a macrophage membrane coated reactive oxygen species (ROS)-responsive nanoparticles (NPs)-derived drug delivery system [16]. Kong et al. comprehensively explained the cascade activation mechanism of the NLRP3 inflammasome signaling pathway and proposed treating AS by targeting key inflammatory pathways [17]. New photodynamic therapy technologies like nanomotor driven methods, can better target endothelial cells, achieving precision drug delivery and treatment [18–21]. Sun's team recently identified the endogenous receptors CYSLTR2 and P2RY6 for ceramide. They revealed that ceramide exacerbates atherosclerosis and chronic kidney disease by activating these receptors and inflammasomes, offering new targets for managing lipid metabolism disorders and residual lipid risk [22]. In addition, laser technology shows great potential in AS diagnosis and treatment. Intravascular optical coherence tomography (IVOCT) combines time-domain (TD) and Fourier-domain (FD) techniques, while intravascular photoacoustic imaging (IVAP) integrates optical excitation and acoustic signal detection to significantly enhance micrometer-level resolution for identifying plaque component [23]. The excimer laser uses ultraviolet light to break molecular bonds in AS lesion plaques, reducing them to small particles [24,25]. However, traditional laser therapy lacks molecular targeting and poses a risk of thermal damage to surrounding tissues. Moreover, stent and catheter implantation during the procedure may also lead to new issues such as vascular intimal hyperplasia and thrombosis [23,25].

This study proposes a new method for laser-targeted therapy based on photon-phonon resonant absorption (PPRA). We select four typical cholesterol esters, which are important components of lipid plaques: cholesterol linoleate (CLA), cholesterol oleate (COA), cholesterol palmitate (CPA), and cholesterol stearate (CSA). The infrared (IR) and Raman spectra of these esters were calculated by using first-principles methods, and the vibrational modes were assigned accordingly. This work offers a theoretical basis and a new direction for the precise laser intervention therapy of AS.

2. Methods

As solid cholesteryl esters are amorphous in structural growth, simulating their intermolecular interactions requires a huge supercell. Besides, their IR and Raman spectra have no characteristic peaks in the hydrogen-bonding regions. Thus, four single-molecule models were used to study their intramolecular vibrational modes. The DMoL^3 code of the first-principles density functional theory (DFT) was employed to perform geometric optimization and vibrational spectrum simulation [26]. It is found that the Perdew–Burke–Ernzerhof exchange-correlation functional (PBE) is more accurate in calculating the vibrational spectrums of cholesteryl esters [27]. The convergence tolerance was set to 1×10^{-5} Ha and the self-consistent field convergence criterion was set to 1×10^{-9} eV/atom. We selected DNP with the DSPP pseudopotential as the basis set, and the energy cutoff was 3.7 Å. Based on the harmonic approximation, the dynamic processes of all vibrational modes for four cholesteryl esters were analyzed. This enabled us to assign the reported experimental peaks and identify the vibrational modes with strong photon–phonon coupling.

3. Results and Discussion

The cholesteryl ester is structurally composed of the cyclopentaphenanthrene ring system, which is attached to the aliphatic hydrocarbon by an ester bond at the third position of the steroid [3]. Specifically, the fatty acid of CLA ($C_{45}H_{76}O_2$) is linoleic acid with 18 carbon atoms and two cis C=C bonds, showing a di-unsaturated feature. That of COA ($C_{45}H_{78}O_2$) is also an 18-carbon unsaturated fatty acid with a single cis C=C bond. CPA ($C_{43}H_{76}O_2$) contained a 16- carbon saturated palmitic acid with no C=C bonds and CSA ($C_{45}H_{80}O_2$) is combined with an 18-carbon saturated stearic acid. Common specific structural formulas of the four cholesteryl esters are shown in Figure 1. It

 doi:10.20944/preprints202505.0475.v1

could be found that their differences mainly lie in the length of the fatty acid chain, the degree of unsaturation, the number and position of C=C bonds. A single molecule of CLA contains 123 atoms, which means there are $123 \times 3 - 3 = 366$ vibrational modes that can be detected by IR and Raman spectra. Similarly, COA, CPA, and CSA have 372, 360, and 378 vibrational modes, respectively. However, the intensity of each peak in IR and Raman spectra may vary depending on the selection rules. Therefore, we focused on the characteristic IR peaks with high PPRA and used the Raman peaks for validation.

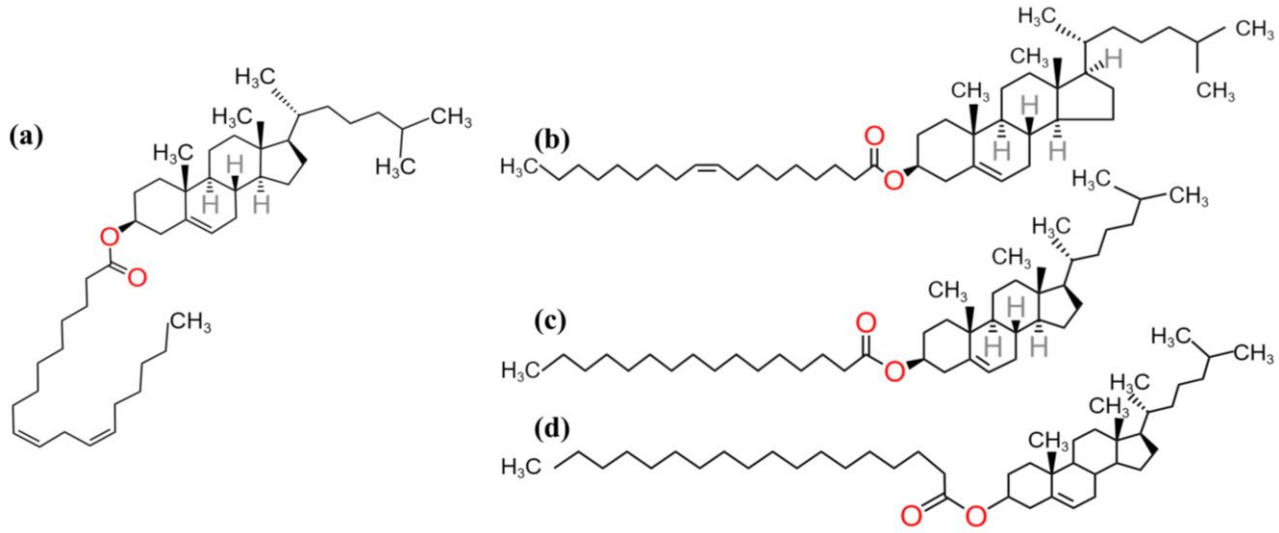

Figure 1. The structural formulas of four cholesteryl esters: CLA (a), COA (b), CPA (c), CSA (d).

Figure 2 presents the simulated IR and Raman spectra of four cholesteryl esters (CLA, COA, CPA, CSA). Through dynamic analysis of the vibrational modes, we classified them into four energy bands, which were skeletal vibrations, C–H bending vibrations, C=C/C=O stretching vibrations, and C–H stretching vibrations. Vibrations with wavenumbers below $500\ cm^{-1}$, which involve complex motions of carbon chains and cooperative skeletal deformations, were assigned to skeletal vibrations. A sharp peak observed at around $430\ cm^{-1}$ in the Raman spectra in pervious experiments was attributed to the CH_2 deformation in the ring, which was considered as one of the cholesterol backbone marker bands [28,29]. Here we observed similar vibrations at $450\ cm^{-1}$ (CLA), $439\ cm^{-1}$ (COA), $461\ cm^{-1}$ (CPA) and $435\ cm^{-1}$ (CSA). Dynamic analysis indicated these modes correspond to cooperative deformations of CH_2/CH_3 groups near the cholesterol benzene ring and the benzene ring skeleton as shown in Figure 3.

 doi:10.20944/preprints202505.0475.v1

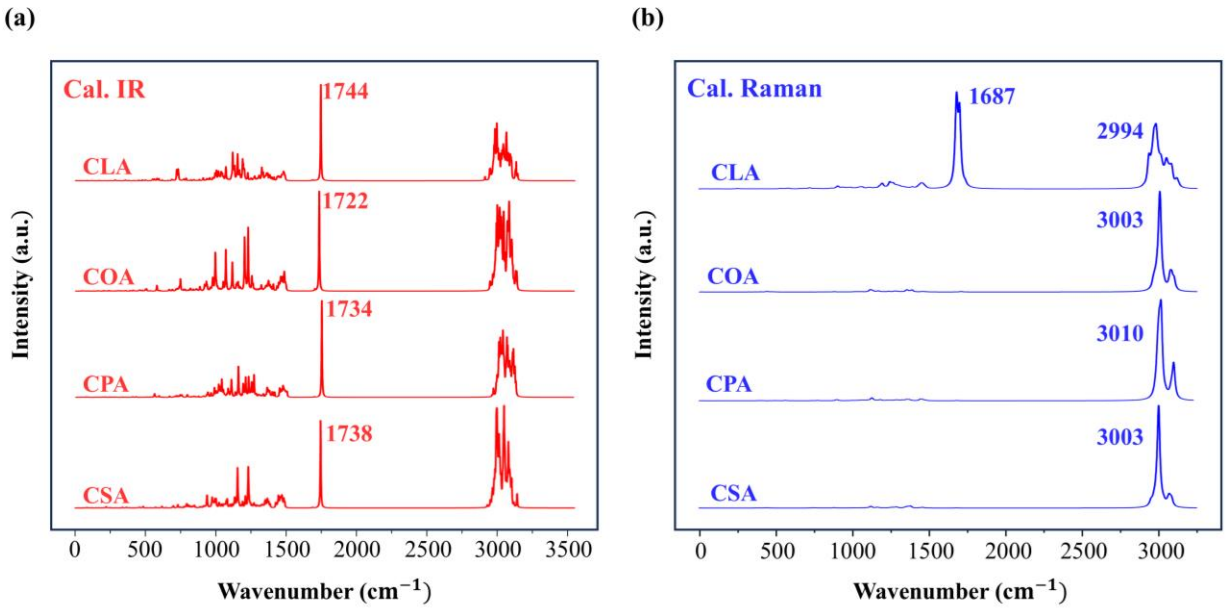

Figure 2. The calculated IR (a) and Raman spectra (b) of the four cholesteryl esters: CLA, COA, CPA, CSA.

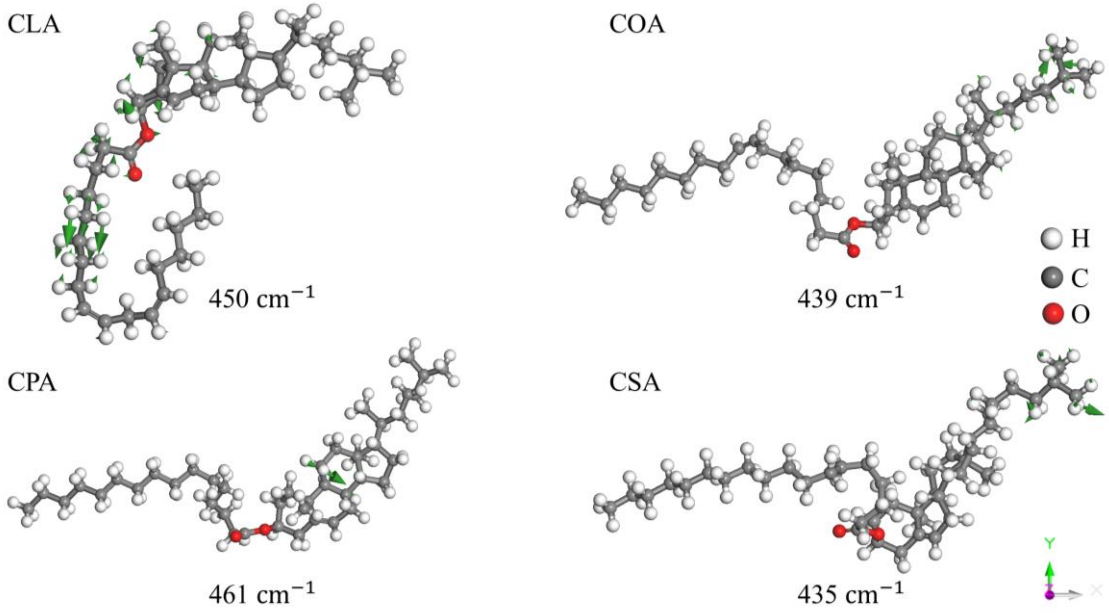

Figure 3. Four kinds of the complex skeletal vibrational modes of CLA, COA, CPA, and CSA. Green arrows indicate the motion direction of atoms in proportional with the amplitude.

The vibrational modes in the range from 500 to 1600 cm^{-1} involving various dihedral angle deformations of C–H bonds were assigned to C–H bending vibrations. The calculated IR spectra of the four cholesteryl esters showed many peaks in this region. We observed distinct vibrational peaks at around 720 cm^{-1} in IR spectra of CLA and COA, with similar modes detected in the other two cholesterol esters. We presented four vibrational modes at 719 cm^{-1} (CLA), 740 cm^{-1} (COA), 736 cm^{-1} (CPA), and 727 cm^{-1} (CSA) as shown in Figure 3. Iyengar et al. classified the peak near 720 cm^{-1} as the rocking vibration of the CH_2 groups in the lipid chain [30,31]. In this work, for unsaturated CLA and COA, they were attributed to H–C=C–H rocking vibrations, whereas those for saturated CSA and CPA, they originated from CH_2 rocking vibrations. We observed two strong vibrational peaks of CLA at 719 cm^{-1} and 729 cm^{-1}, which correspond to the out-of-plane bending vibration of the H–C=C–C–H groups. For unsaturated cholesteryl esters CLA and COA, the presence

 doi:10.20944/preprints202505.0475.v1

of the H-C=C-H groups in their fatty acid chains leads to a greater degree of freedom, resulting in stronger corresponding vibrational peaks in this region. Smith identified strong ester peaks at around 1100cm^{-1}, and 1200 cm^{-1}, corresponding to C–C–O and O–C–C stretching vibration, respectively [32]. Wrobel et al. also noted that the absorption peaks in the $1160-1175$ cm^{-1} region were originated from the C–O–C stretching vibrations, which were only found in esters and not in fatty acids or cholesterol, could be a standard for distinguishing esters from alcohols and acids [31]. In contrast, our analysis of four strong IR peaks at 1188 cm^{-1} (CLA), 1195cm^{-1} (COA), 1145 cm^{-1} (CPA), and 1150 cm^{-1} (CSA) as shown in Figure 5, indicated that these vibrations are primarily attributed to bending vibrations of CH_2 groups near the ester group, accompanied by C–O stretching vibrations. Ignored these details, our theoretical analysis classified as CH_2 bending modes in this band. Broad peaks in the $1400-1500$ cm^{-1} region are observed in IR spectra of the four esters. These modes are identified as C–H bending vibrations of CH_2/CH_3 groups too. Experimental studies have reported Raman peaks near 1440 cm^{-1} cholesterol esters and IR peaks near 1470 cm^{-1}, attributed to CH_2/CH_3 scissoring and bending vibrations [28–31].

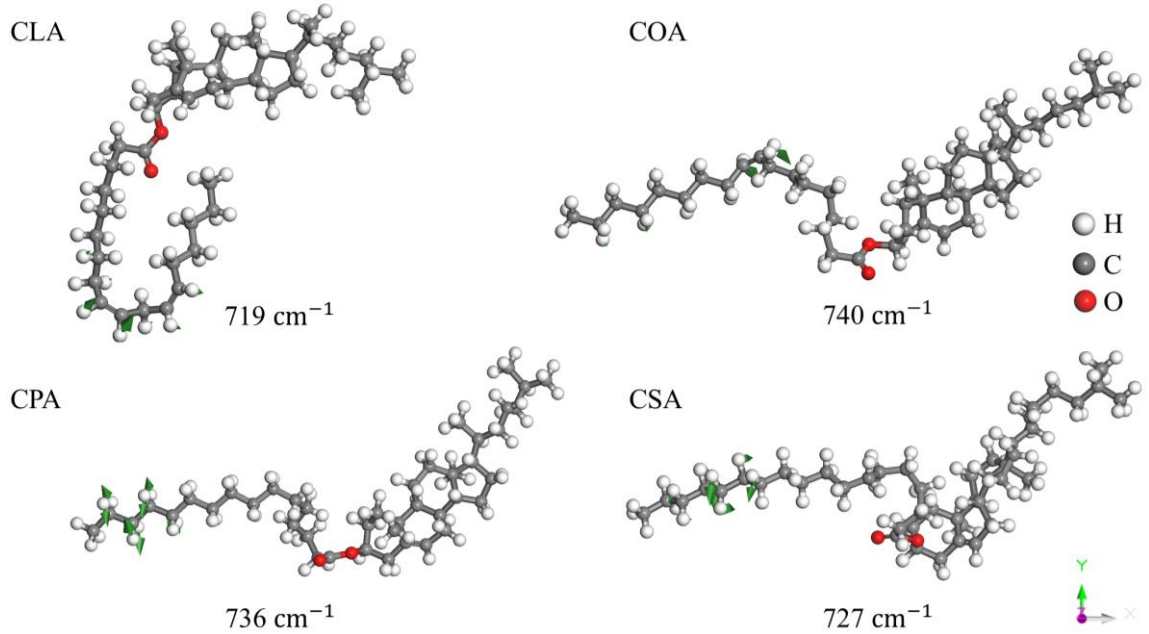

Figure 4. Four vibrational modes at around 720 cm^{-1}. The wavenumbers at 719 and 740 cm^{-1} show H–C=C–H rocking and the other two show CH_2 rocking in the FA chain.

 doi:10.20944/preprints202505.0475.v1

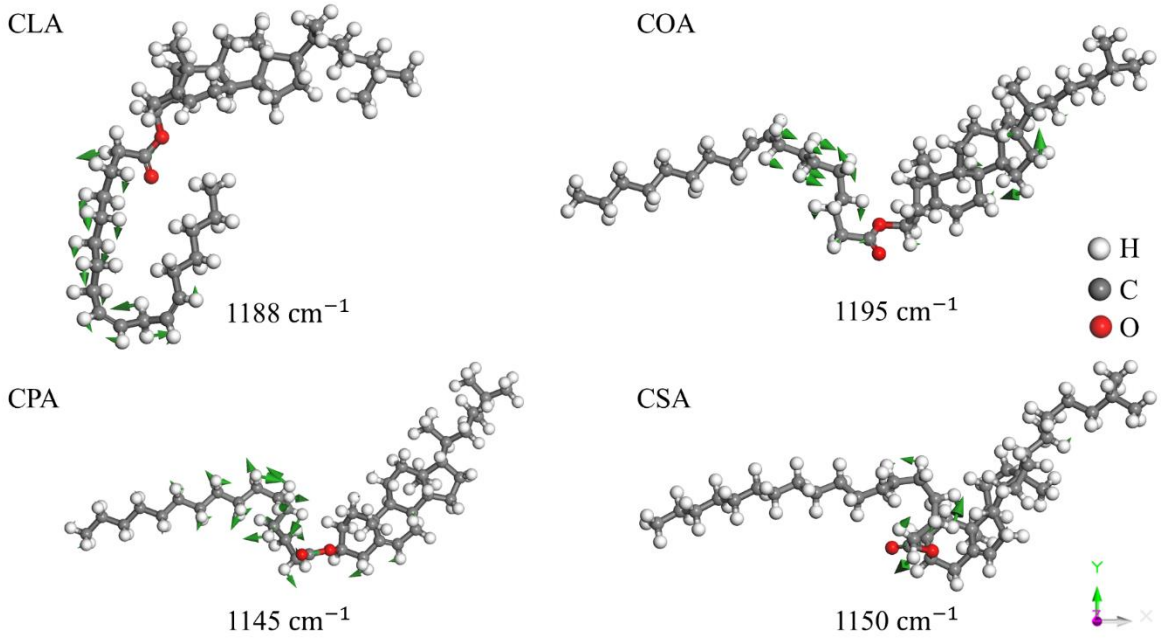

Figure 5. Four examples of C-H bending vibrations of CLA, COA, CPA, and CSA in the region from 1100 cm^{-1} to 1200 cm^{-1}.

CLA has a special peak at around 1690 cm^{-1} in the Raman spectrum, which is distinct from other cholesteryl esters. Analysis of this vibrational mode revealed that there were two modes at 1682 $cm^{-1}$and 1687 cm^{-1}, which originate from the asymmetric and symmetric stretching vibrations of two C=C bonds in the FA chain. And there was a vibrational mode at 1707 cm^{-1} corresponding to the stretching vibration of C=C bond in the benzene ring. The three vibrational modes are depicted in Figure 6. The coupling effect of these C=C vibrational modes results in a strong, narrow-bandwidth Raman peak of CLA. For COA, which is also unsaturated, the C=C stretching vibrations were observed at 1706 cm^{-1} in the FA chain and at 1692 cm^{-1} in the benzene ring. The saturated CPA and CSA has only one C=C in the benzene ring, corresponding to the vibrations at 1680 cm^{-1} and 1681cm^{-1}, respectively. The reported experimental C=C vibrations occured at $1660-1680$ cm^{-1} [28,30,33], and the theoretical results here show slightly blue shifts.

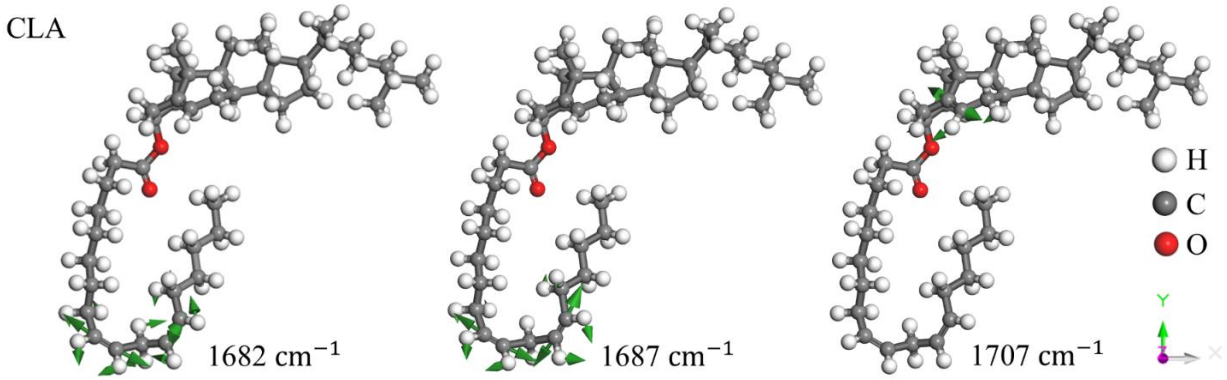

Figure 6. Three kinds of C=C stretching vibrations of CLA. The first two show asymmetric and symmetric stretching of C=C in the FA chain, and the third shows C=C stretching in the benzene ring.

There is a dominant peak at 1744, 1722, 1734, and 1738 cm^{-1} respectively in the simulated IR spectra of these four cholesterol esters corresponding to C=O stretching vibration as shown in Figure 7, which matches the reported experimental result [30,31,34–36]. It can be concluded that the

 doi:10.20944/preprints202505.0475.v1

C=O stretching vibrations of cholesteryl esters are in the range from 1720 to 1750 cm^{-1}, independent of the carbon chain length [37]. For the dynamic process, please see the supplementary file. The other strong peaks near 3000 cm^{-1} exhibit notable bandwidth features, mainly arising from C–H stretching vibrations of CH_2/CH_3 groups, aligning with previous lipid characteristic reports [28–31,36]. Some experiments have assigned the vibrations near $2850-2900\ cm^{-1}$ and $2900-2950\ cm^{-1}$ to the symmetric and asymmetric stretching vibrations of CH_2 and CH_3, respectively [30,31]. However, the calculated vibrational modes were limited in the range of $2900-3200\ cm^{-1}$. Analysis revealed that the vibrational modes at $2950-3000\ cm^{-1}$ are primarily due to symmetric stretching of C–H bonds in CH_2/CH_3 groups, while peaks at $3000-3200\ cm^{-1}$ mainly originate from asymmetric stretching of C–H bonds in CH_2/CH_3 groups of the FA chain, as shown in Figure 8, which shows specific differences from previous experiments. Additionally, in the IR spectra of CSA, the intensity of C–H vibrations is slightly stronger than that of C=O vibrations. This may be attributed to its longer carbon chain with more CH_2 units and a saturated FA chain without C=C restrictions.

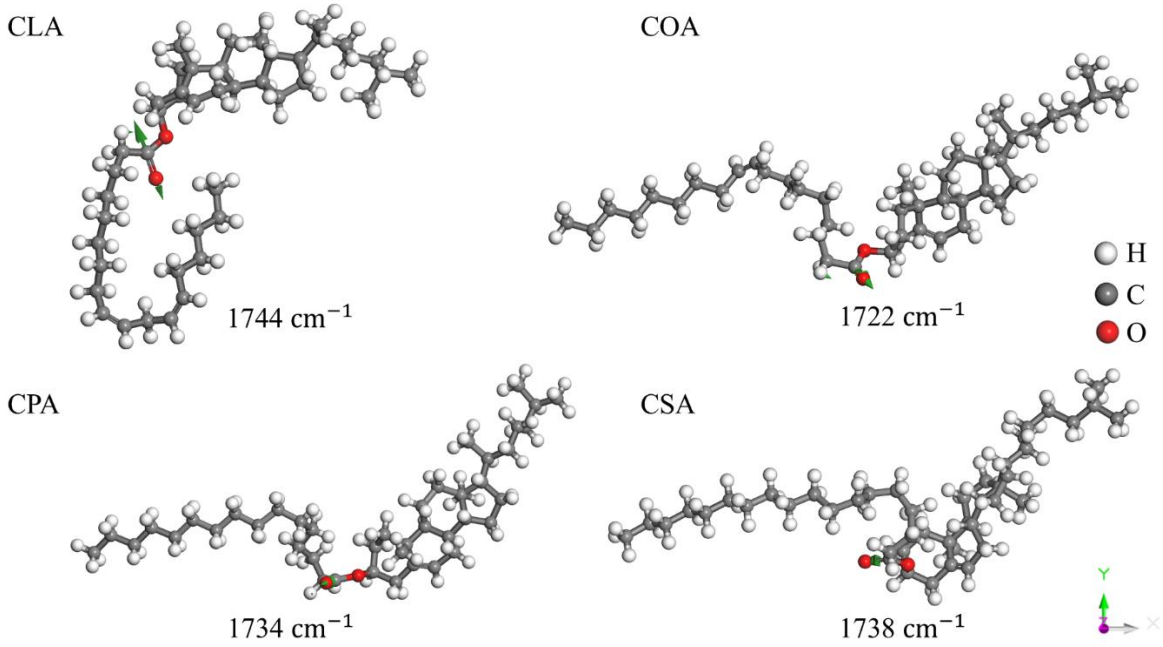

Figure 7. Four C=O stretching vibration modes of CLA, COA, CPA, and CSA. These modes show strong IR absorption peaks.

 doi:10.20944/preprints202505.0475.v1

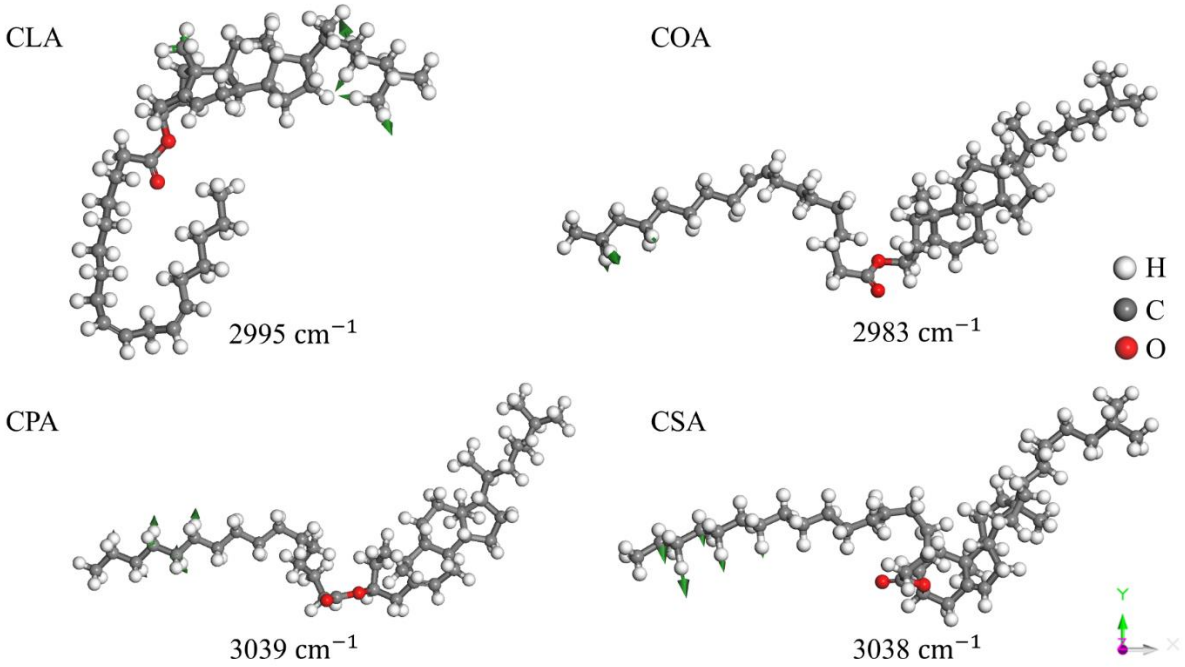

Figure 7. Examples of C–H stretching vibrational modes of CLA, COA, CPA, and CSA.

The calculated IR and Raman spectra in this study show certain differences in the characteristic peaks of the fingerprint region compared to the previously reported experimental spectra, which is mainly attributed to the simplification of theoretical models. These calculations were based on monomolecular model, ignoring the molecular environment and intermolecular non-covalent interactions. Thus, the positions or intensities of peaks in the fingerprint region, which are sensitive to intermolecular interactions, may be quite different. However, the strong IR peaks originated from C=O vibrations presented good agreement with the experimental reports. It is located in the range of $1720 - 1750\ \mathrm{cm}^{-1}$, i.e. 52 THz.

In this paper, we mainly focus on the C=O vibration peaks which exhibit high PPRA efficiency. In principle, the IR signals are due to photon-phonon resonance absorption while the Raman scattering signals are different frequency photon-phonon coupling. Since the light intensity of Raman scattering is 10^{-7} lower than that of IR, it is obviously that the best photothermal effect rely on the matchable frequencies between photon and phonon. Provided a laser of which the frequency is at around 52 THz focuses on the plaque, the C=O vibrations will obtain energy level transitions quickly. On the other way, the high electronegativity of C=O enables this group to participate in the stable formation of intermolecular hydrogen bond networks. The high vibrational energy of C=O bond may facilitate the hydrogen bonds breaking, and then destabilize the hydrophobic core of the lesion plaque and induce the phase transition of ester components from solid or liquid crystalline states to a liquid state. This disruption also affects unsaturated cholesteryl ester lipid droplets by weakening intermolecular forces and reducing viscosity. Cholesterol ester molecules experience reduced volume and increased mobility after phase transition, making them more susceptible to hydrolysis by esterases and subsequent excretion from the cell. This process consequently accelerates reverse cholesterol transport and diminishes lipid deposition within the vessel wall, thereby alleviating atherosclerosis.

3. Conclusions

In this study, we use first-principles DFT method to simulate the IR and Raman spectra of four types of cholesteryl esters to investigate their structures and properties. The calculated vibrational modes were assigned into five corresponding types: skeletal vibrations ($< 500\ \mathrm{cm}^{-1}$), C–H bending

 doi:10.20944/preprints202505.0475.v1

vibrations ($500-1600\ cm^{-1}$), C=C stretching vibrations ($1600-1700\ cm^{-1}$), C=O stretching vibrations ($1700-1800\ cm^{-1}$), and C–H stretching vibrations ($2900-3200\ cm^{-1}$). Compared to previous experiments, the distributions of vibrational modes in the computed spectral fingerprint region show slight differences. However, the positions of the C=O stretching vibration remain consistent ($1720-1750\ cm^{-1}$). This vibrational mode is stably present in all four types of cholesterol esters, regardless of their carbon chain lengths. We theoretically suggested to use a 52 THz laser, matching the C=O vibration frequency, to irradiate atherosclerotic lesions. The real precise frequency and bandwidth need further experimental tests. It is predicted to induce lipid plaque phase transitions, accelerate cholesteryl ester hydrolysis and plaque ablation through efficient PPRA.

It is important to note that atherosclerotic plaques also contain various other substances, such as proteins and phospholipids. Furthermore, precise control of the laser focusing intensity and irradiation sites in vivo requires rigorous techniques and repeated experimental testing. Nevertheless, this work provides a novel theoretical framework and research direction for laser-targeted therapies.

Supplementary Materials: The following supporting information can be downloaded at the website of this paper posted on Preprints.org, Video S1: The dynamic process of vibrational mode at 1744 cm^{-1}.

Author Contributions: Y.W. was mainly responsible for the model construction and article writing; P.L. and H.R. assisted with the structural modelling; Y.L. (Yining Li), Y.L. (Yawen Li), J.Z. and Y.X. participated in the discussion of the results; and P.Z. conducted the simulations and edited the manuscript. All authors have read and agreed to the published version of the manuscript.

Funding: The authors are grateful to the project ZR2022MA017, supported by Shandong Provincial Natural Science, for providing financial support.

Data Availability Statement: Data are available from the authors on request.

Acknowledgments: The numerical calculations were performed on the supercomputing system at the Supercomputing Center of Shandong University, Weihai.

Conflicts of Interest: The authors declare no conflicts of interest.

References

1. Jebari-Benslaiman, S.; Galicia-García, U.; Larrea-Sebal, A.; Olaetxea, J. R.; Alloza, I.; Vandenbroeck, K.; Benito-Vicente, A.; Martín, C. Pathophysiology of atherosclerosis. *International Journal of Molecular Sciences* **2022**, *23*, 3346. https://doi.org/10.3390/ijms23063346.
2. Hevonoja, T.; Pentikäinen, M. O.; Hyvönen, M. T.; Kovanen, P. T.; Ala-Korpela, M. Structure of low density lipoprotein (LDL) particles: Basis for understanding molecular changes in modified LDL. *Biochimica Et Biophysica Acta (BBA) - Molecular and Cell Biology of Lipids* **2000**, *1488*, 189–210. https://doi.org/10.1016/s1388-1981(00)00123-2.
3. Ginsburg, G. S.; Atkinson, D.; Small, D. M. Physical properties of cholesteryl esters. Progress in Lipid Research 1984, 23 (3), 135–167. https://doi.org/10.1016/0163-7827(84)90002-x.
4. Chistiakov, D. A.; Melnichenko, A. A.; Myasoedova, V. A.; Grechko, A. V.; Orekhov, A. N. Mechanisms of foam cell formation in atherosclerosis. *Journal of Molecular Medicine* **2017**, *95*, 1153–1165. https://doi.org/10.1007/s00109-017-1575-8.
5. Fan, J.; Watanabe, T. Atherosclerosis: Known and unknown. *Pathology International* **2022**, *72*, 151–160. https://doi.org/10.1111/pin.13202.
6. Zmysłowski, A.; Szterk, A. Current knowledge on the mechanism of atherosclerosis and pro-atherosclerotic properties of oxysterols. *Lipids in Health and Disease* **2017**, *16*. https://doi.org/10.1186/s12944-017-0579-2.
7. Björkegren, J. L. M.; Lusis, A. J. Atherosclerosis: Recent developments. *Cell* **2022**, *185*, 1630–1645. https://doi.org/10.1016/j.cell.2022.04.004.

 doi:10.20944/preprints202505.0475.v1

8. Libby, P. The changing landscape of atherosclerosis. *Nature* **2021**, *592*, 524–533. https://doi.org/10.1038/s41586-021-03392-8.
9. Hetherington, I.; Totary-Jain, H. Anti-atherosclerotic therapies: Milestones, challenges, and emerging innovations. *Molecular Therapy* **2022**, *30*, 3106–3117. https://doi.org/10.1016/j.ymthe.2022.08.024.
10. Almeida, S. O.; Budoff, M. Effect of statins on atherosclerotic plaque. *Trends in Cardiovascular Medicine* **2019**, *29*, 451–455. https://doi.org/10.1016/j.tcm.2019.01.001
11. Engelen, S. E.; Robinson, A. J. B.; Zurke, Y.-X.; Monaco, C. Therapeutic strategies targeting inflammation and immunity in atherosclerosis: how to proceed? *Nature Reviews Cardiology* **2022**, *19*, 522–542. https://doi.org/10.1038/s41569-021-00668-4.
12. Thompson, P. D.; Panza, G.; Zaleski, A.; Taylor, B. Statin-Associated side Effects. Journal of the American College of Cardiology **2016**, *67*, 2395–2410. https://doi.org/10.1016/j.jacc.2016.02.071.
13. Poznyak, A. V.; Bharadwaj, D.; Prasad, G.; Grechko, A. V.; Sazonova, M. A.; Orekhov, A. N. Anti-Inflammatory therapy for atherosclerosis: Focusing on cytokines. *International Journal of Molecular Sciences* **2021**, *22*, 7061. https://doi.org/10.3390/ijms22137061.
14. Luo, T.; Zhang, Z.; Xu, J.; Liu, H.; Cai, L.; Huang, G.; Wang, C.; Chen, Y.; Xia, L.; Ding, X.; Wang, J.; Li, X. Atherosclerosis treatment with nanoagent: potential targets, stimulus signals and drug delivery mechanisms. *Frontiers in Bioengineering and Biotechnology* **2023**, *11*. https://doi.org/10.3389/fbioe.2023.1205751.
15. Chen, W.; Schilperoort, M.; Cao, Y.; Shi, J.; Tabas, I.; Tao, W. Macrophage-targeted nanomedicine for the diagnosis and treatment of atherosclerosis. *Nature Reviews Cardiology* **2021**, *19*, 228–249. https://doi.org/10.1038/s41569-021-00629-x.
16. Gao, C.; Huang, Q.; Liu, C.; Kwong, C. H. T.; Yue, L.; Wan, J.-B.; Lee, S. M. Y.; Wang, R. Treatment of atherosclerosis by macrophage-biomimetic nanoparticles via targeted pharmacotherapy and sequestration of proinflammatory cytokines. *Nature Communications* **2020**, *11*. https://doi.org/10.1038/s41467-020-16439-7.
17. Kong, P.; Cui, Z.-Y.; Huang, X.-F.; Zhang, D.-D.; Guo, R.-J.; Han, M. Inflammation and atherosclerosis: signaling pathways and therapeutic intervention. *Signal Transduction and Targeted Therapy* **2022**, *7*. https://doi.org/10.1038/s41392-022-00955-7.
18. Li, X.; Wu, R.; Chen, H.; Li, T.; Jiang, H.; Xu, X.; Tang, X.; Wan, M.; Mao, C.; Shi, D. Near-Infrared Light-Driven multifunctional tubular micromotors for treatment of atherosclerosis. *ACS Applied Materials & Interfaces* **2021**, *13*, 30930–30940. https://doi.org/10.1021/acsami.1c03600.
19. Tang, X.; Chen, L.; Wu, Z.; Li, Y.; Zeng, J.; Jiang, W.; Lv, W.; Wan, M.; Mao, C.; Zhou, M. Lipophilic NO-Driven nanomotors as drug balloon coating for the treatment of atherosclerosis. *Small* **2022**, *19*. https://doi.org/10.1002/smll.202203238.
20. Wu, Z.; Zhou, M.; Tang, X.; Zeng, J.; Li, Y.; Sun, Y.; Huang, J.; Chen, L.; Wan, M.; Mao, C. Carrier-Free Trehalose-Based nanomotors targeting macrophages in inflammatory plaque for treatment of atherosclerosis. *ACS Nano* **2022**, *16*, 3808–3820. https://doi.org/10.1021/acsnano.1c08391.
21. Lee, S.-Y.; Kim, J. H.; Song, J. W.; Min, J. S.; Kim, H. J.; Kim, R. H.; Ahn, J. W.; Yoo, H.; Park, K.; Kim, J. W. Macrophage-mannose-receptor-targeted photoactivatable agent for in vivo imaging and treatment of atherosclerosis. *International Journal of Pharmaceutics* **2024**, *654*, 123951. https://doi.org/10.1016/j.ijpharm.2024.123951.
22. Zhang, S.; Lin, H.; Wang, J.; Rui, J.; Wang, T.; Cai, Z.; Huang, S.; Gao, Y.; Ma, T.; Fan, R.; Dai, R.; Li, Z.; Jia, Y.; Chen, Q.; He, H.; Tan, J.; Zhu, S.; Gu, R.; Dong, Z.; Li, M.; Xie, E.; Fu, Y.; Zheng, J.; Jiang, C.; Sun, J.; Kong, W. Sensing ceramides by CYSLTR2 and P2RY6 to aggravate atherosclerosis. *Nature* **2025**. https://doi.org/10.1038/s41586-025-08792-8.
23. Li, J.; Shang, C.; Rong, Y.; Sun, J.; Cheng, Y.; He, B.; Wang, Z.; Li, M.; Ma, J.; Fu, B.; Ji, X. Review on laser technology in intravascular imaging and Treatment. *Aging and Disease* **2022**, *13*, 246. https://doi.org/10.14336/ad.2021.0711.
24. Machowiec, P.; Ręka, G.; Piecewicz-Szczęsna, H. Usage of excimer laser in coronary and peripheral artery stenosis – analysis of its safety aspect. *Journal of Pre-Clinical and Clinical Research* **2020**, *14*, 145–150. https://doi.org/10.26444/jpccr/127732.

 doi:10.20944/preprints202505.0475.v1

25. Nagamatsu, H.; Torii, S.; Aihara, K.; Nakazawa, K.; Nakamura, N.; Noda, S.; Sekino, S.; Yoshimachi, F.; Nakazawa, G.; Ikari, Y. Histological evaluation of vascular changes after excimer laser angioplasty for neointimal formation after bare-metal stent implantation in rabbit iliac arteries. *Cardiovascular Intervention and Therapeutics* **2023**, *38*, 223–230. https://doi.org/10.1007/s12928-022-00905-8.
26. Delley, B. An All-Electron Numerical Method for Solving the Local Density Functional for Polyatomic Molecules. J. *Chem. Phys.* **1990**, *92*, 508−517. https://doi.org/10.1063/1.458452.
27. Perdew, J. P.; Burke, K.; Wang, Y. Generalized Gradient Approximation for the Exchange-Correlation Hole of a Many-Electron System. *Phys. Rev. B Condens. Matter* **1996**, *54*, 16533–16539. https://doi.org/10.1103/physrevb.54.16533.
28. Czamara, K.; Majzner, K.; Pacia, M. Z.; Kochan, K.; Kaczor, A.; Baranska, M. Raman spectroscopy of lipids: a review. *Journal of Raman Spectroscopy* **2014**, *46*, 4–20. https://doi.org/10.1002/jrs.4607.
29. Krafft, C.; Neudert, L.; Simat, T.; Salzer, R. Near infrared Raman spectra of human brain lipids. *Spectrochimica Acta Part a Molecular and Biomolecular Spectroscopy* **2004**, *61*, 1529–1535. https://doi.org/10.1016/j.saa.2004.11.017.
30. Iyengar, S. R.; Prasad, J. S.; Venkataraman, S. Vibrational spectra of sterol and non-sterol cholesterogens. *Molecular Crystals and Liquid Crystals* **1987**, *146*, 265–285. https://doi.org/10.1080/00268948708071818.
31. Wrobel, T. P.; Mateuszuk, L.; Chlopicki, S.; Malek, K.; Baranska, M. Imaging of lipids in atherosclerotic lesion in aorta from ApoE/LDLR−/− mice by FT-IR spectroscopy and Hierarchical Cluster Analysis. *The Analyst* **2011**, *136*, 5247. https://doi.org/10.1039/c1an15311k.
32. Smith, B. C. The C=O Bond, Part VI: Esters and the Rule of Three. *Spectroscopy Online.* December 20, **2020**. https://www.spectroscopyonline.com/view/co-bond-part-vi-esters-and-rule-three.
33. Bresson, S.; Marssi, M. E.; Khelifa, B. First investigations of two important components of low density lipoproteins by Raman spectroscopy: the cholesteryl linoleate and arachidonate. *Vibrational Spectroscopy* **2004**, *34*, 231–241. https://doi.org/10.1016/j.vibspec.2003.11.003.
34. Nara, M.; Okazaki, M.; Kagi, H. Infrared study of human serum very-low-density and low-density lipoproteins. Implication of esterified lipid C=O stretching bands for characterizing lipoproteins. *Chemistry and Physics of Lipids* **2002**, *117*, 1–6. https://doi.org/10.1016/s0009-3084(02)00003-8.
35. Rambharose, S.; Kalhapure, R. S.; Jadhav, M.; Govender, T. Exploring unsaturated fatty acid cholesteryl esters as transdermal permeation enhancers. *Drug Delivery and Translational Research* **2017**, *7*, 333–345. https://doi.org/10.1007/s13346-017-0360-0.
36. Labarrere, J. A.; Chipault, J. R.; Lundberg, W. O. Cholesteryl esters of Long-Chain fatty acids. infrared spectra and separation by paper chromatography. *Analytical Chemistry* **1958**, *30*, 1466–1470. https://doi.org/10.1021/ac60141a008.
37. Li, P.; Li, Y.; Li, Y.; Zhang, J.; Wen, Z.; Zhang, P. Theoretical investigation of a new physical method for fat removal by melting: A case study of caprate triglyceride. *ACS Omega* **2025**, 10, 11354–11358. https://doi.org/10.1021/acsomega.4c11242.